Photodissociation dynamics of indole in a molecular beam

Ming-Fu Lin, Chien-Ming Tseng, Yuan T. Lee,[a] and Chi-Kung Ni[b]
Institute of Atomic and Molecular Sciences, Academia Sinica, P. O. Box 23-166, Taipei, 10617 Taiwan

(Received 11 May 2005; accepted 7 July 2005; published online 26 September 2005)

Photodissociation of indole at 193 and 248 nm under collision-free conditions has been studied in separate experiments using multimass ion imaging techniques. H atom elimination was found to be the only dissociation channel at both wavelengths. The photofragment translational energy distribution obtained at 193 nm contains a fast and a slow component. Fifty-four percent of indole following the 193 nm photoexcitation dissociate from electronically excited state, resulting in the fast component. The rest of 46% indole dissociate through the ground electronic state, giving rise to the slow component. A dissociation rate of 6×10^5 s^{-1}, corresponding to the dissociation from the ground electronic state, was determined. Similar two-component translational energy distribution was observed at 248 nm. However, more than 80% of indole dissociate from electronically excited state after the absorption of 248 nm photons. A comparison with the potential energy surfaces from the *ab initio* calculation has been made. © *2005 American Institute of Physics*. [DOI: 10.1063/1.2009736]

I. INTRODUCTION

Tryptophan fluorescence is widely used for characterizing the structure and dynamics of the surrounding protein environment. The importance of the research on the electronic structure and dynamics of indole stems from the fact that indole is a chromophore of the amino acid tryptophan. Indole has two absorption bands in the near UV, which can be assigned as $\pi^*\leftarrow\pi$ singlet–singlet transitions. The two excited states are labeled by ^1L_a and ^1L_b following the suggestion of Platt.[1] The ^1L_b state lies about 1400 cm^{-1} below ^1L_a. The ^1L_b state has a very strong 0_0^0 transition at 35 232 cm^{-1}.[2–5] The S_0-S_1 origin transition is ascribed to the ^1L_b upper state. The ^1L_a and ^1L_b states have been used to explain most of the observed photophysics of indole.

However, in order to explain the anomalous increase in nonradiative decay of gas phase indole with excess energy above the ^1L_b origin, Glasser and Lami suggested that ^1L_a state undergoes efficient N–H bond fission under collision-free conditions.[6] A model in which ^1L_a and ^1L_b couple to a dissociative state was proposed.[7] In addition, the generation of NH_4-$(NH_3)_n$ from UV-excited indole-$(NH_3)_n$ clusters was described as the photoproducts of intracluster hydrogen atom transfer reactions. The source of H atom was proposed to result from H atom elimination of indole in the excited state.[8] Theoretical calculation from the complete active space self consistent field supported the existence of a third dissociative excited state, $\pi\sigma^*$, located about 0.5 eV above the S_1 state.[9,10] This state is calculated to be dissociative along the NH coordinate. Recently, the study of infrared spectra in the electronically excited states of indole, indole-H_2O, 3-methyl indole, and 3-methyl-indole-H_2O indicates the existence of the $\pi\sigma^*$ state above ^1L_a.[11] However, there is little direct evidence of this state yet.

In this work, we study the photodissociation of indole at 248 and 193 nm using multimass ion imaging techniques. Direct evidence of the H atom elimination from the excited electronic state was reported.

II. EXPERIMENT

The experiments have been described in detail elsewhere,[12–14] and only a brief description is given here. Indole vapor was formed by flowing ultrapure Ne at pressure of 400 Torr through a reservoir filled with solid sample at 55 °C. The indole/Ne mixture was then expanded through a 800 μm high temperature (110 °C) pulsed nozzle to form the molecular beam. Molecules in the molecular beam were photodissociated by a UV photolysis laser pulse (Lambda Physik Compex 205; pulse duration: ~20 ns). Due to the recoil velocity and center-of-mass velocity, the fragments expanded to a larger sphere on their flight to the VUV laser beam path, and then were ionized by a VUV laser pulse. The distance and time delay between the VUV laser pulse and the photolysis laser pulse were set such that the VUV laser beam passed through the center-of-mass of the dissociation products, and generated the photofragment ions along the VUV beam path by photoionization. The length of the segment was proportional to the fragment recoil velocity in the center-of-mass frame multiplied by the delay time between the photolysis and the ionization laser pulses. To separate the different masses within the ion segment, a pulsed electric field was used to extract the ions into a mass spectrometer after ionization. While the mass analysis was being executed in the mass spectrometer, the length of each fragment ion segment continued to expand in the original direction according to its recoil velocity. At the exit port of the mass spectrometer, a two-dimensional ion detector was used to

[a]Also at Department of Chemistry, National Taiwan University, Taipei, Taiwan.
[b]Author to whom correspondence should be addressed. Also at Department of Chemistry, National Tsing Hua University, Hsinchu, Taiwan. Electronic mail: ckni@po.iams.sinica.edu.tw

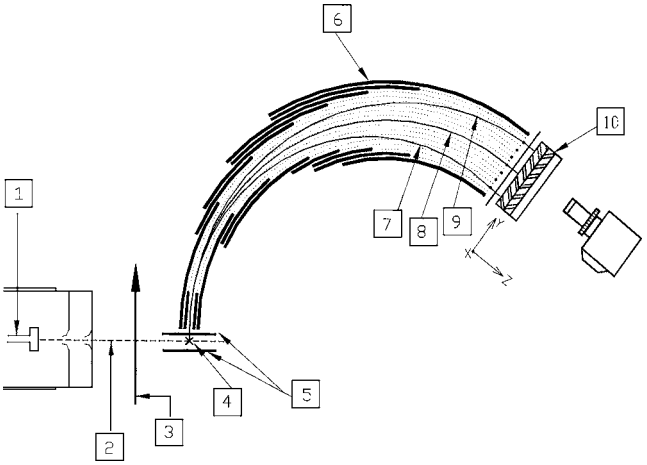

FIG. 1. Schematic diagram of the multimass ion imaging detection system. (1) nozzle; (2) molecular beam; (3) photolysis laser beam; (4) VUV laser beam, which is perpendicular to the plane of the paper; (5) ion extraction plates; (6) cylindrical energy analyzer; (7), (8), and (9) simulation ion trajectories of $m/e=16$, 14, 12; (10) two-dimensional detector, where Y-axis is mass axis, and X-axis (perpendicular to the plane of the paper) is the velocity axis.

detect the ion positions and intensity distribution. In this two-dimensional detector, one direction was the recoil velocity axis and the other was the mass axis. The schematic diagram of the experimental set up is shown in Fig. 1.

Depending on the velocity of the molecular beam, it was necessary to change the distance between the photolysis laser beam and the VUV laser beam to match the delay time between these two laser pulses to ensure that the ionization laser would pass through the center-of-mass of the products. The change of the distance between the two laser beams changed the length of the fragment ion segment in the image. The relationship between the length of the ion image and the position of the photolysis laser is illustrated in Fig. 2. If the molecules did not dissociated after the absorption of UV photons, these high internal energy molecules would remain within the molecular beam. They flew with the same velocity (molecular beam velocity) to the ionization region and were ionized by the VUV laser. The wavelength of the VUV laser in this experiment was set at 118.2 nm such that the photon energy was only large enough to ionize parent molecules. The dissociation of parent molecule cations would not occur with the energy left after the VUV laser ionization. However, the dissociation occurred following the VUV laser ionization for those hot molecules, which absorbed UV photon and did not dissociate into fragments before the arrival of the VUV laser pulse. The ion image of the dissociative ionization was different from the image of the dissociation products of neutral parent molecules. Since ionization and dissociation occurred at the same position, the image of dissociative ionization was a 2D projection of the photofragment ion's 3D-recoil velocity distribution. It was a disk-like image, rather than a line-shape image. From the shape of the image and its change with the delay time, the image from dissociation of neutral molecules can easily be distinguished from the dissociative ionization image.

The dissociation rate was measured from the product growth or disk-like image intensity decay as a function of delay time between pump and probe laser pulses.

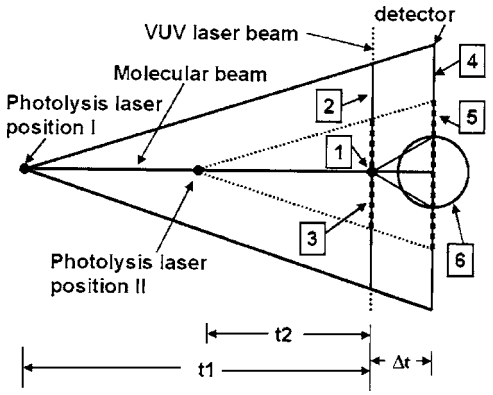

FIG. 2. Relationship between the lengths of the images that results from different crossing points of photolysis laser beam with molecular beam. The disk-like image from the dissociation after ionization is also shown. (1) represents the crossing point of the molecular beam and the VUV laser beam, where the dissociative ionization occurs. The disk-like image, represented by (6) is from the dissociative ionization. (2) and (3) represent the lengths of fragment ion distribution created by VUV laser photoionization from photolysis laser at position I and position II, respectively. The line shape images, represented by (4) and (5), are from these fragment ion distributions (2) and (3). The t_1 and t_2 represent two different delay times between the photolysis laser pulse and the VUV laser pulse according to two different photolysis laser positions. Δt is the flight time of fragment ion in the mass spectrometer.

III. RESULTS

A. 193 nm

Fragment ions, including $m/e=89$, 90, 116, and 117, were observed. Figure 3(a) shows the images of $m/e=89$ and 90. The shapes of the images of m/e=89 and 90 are both disk-like. They overlapped and cannot be separated totally from each other. The widths of the images do not change with the delay time between pump and probe laser pulses, as illustrated in Fig. 3(b). Therefore, they must result from the dissociation of excited indole after ionization.

Figure 4 shows the images in the mass range from $m/e=114$ to 122. The center parts of the images of m/e

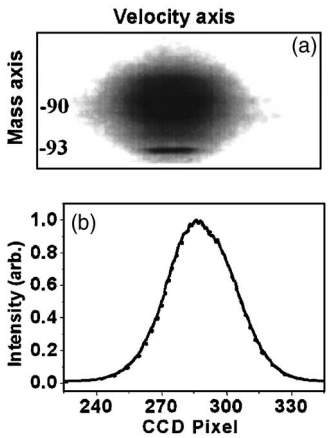

FIG. 3. (a) Ion image of $m/e=89$ and 90. $m/e=93$ was a mass indicator. (b) Image intensity profiles of $m/e=90$ at delay time 7 μs (dotted line) and 13 μs (solid line).

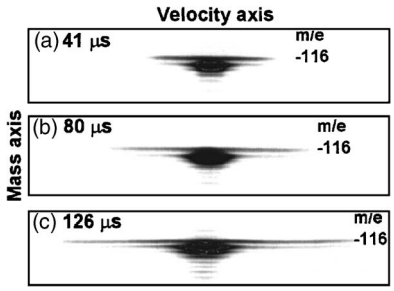

FIG. 4. Ion images in the range of $m/e=114-122$ obtained at various delay times between pump and probe laser pulses.

$=117$, 118, 119, 120 are from the indole parent molecule and its ^{13}C isotopomers due to the ^{13}C natural abundance. Fragment ion $m/e=116(C_8NH_6^+)$ has the largest ion intensity. The images at several different delay times between pump and probe delay pulses are shown in Figs. 4(a)–4(c). A disk-like image superimposed on the center of a line shape image was observed at very short delay time. As the delay time between pump and probe laser pulses increased, the length of the line shape image increased rapidly and the intensity of the disk-like image decreased. The line shape image is the C_8NH_6 fragment that resulted from the dissociation of neutral excited indole, corresponding to the H atom elimination. The line shape image of $m/e=117$ has the same intensity profile as that of $m/e=116$, but the intensity of $m/e=117$ is about 9 % of $m/e=116$. The relative intensity and intensity profiles of $m/e=116$ and 117 indicate that the line shape image on both wings of $m/e=117$ is the ^{13}C isotopomer of $m/e=116$ photofragment.

The photofragment translational energy distribution obtained from the image of $m/e=116$ is shown in Fig. 5. It shows that there are two components. The relative intensities between the fast and the slow components are about 1:0.85. The average released translational energy of the fast component is large, and the peak of the distribution is located at 30 kcal/mol. It is interesting to note that the maximum translational energy reaches the maximum available energy of the reaction $C_8NH_7 \rightarrow C_8NH_6+H(\Delta H=90$ kcal/mol).[15] The distribution indicates that the dissociation must occur through a repulsive potential or from an electronically excited state with a large exit barrier. On the other hand, the average translational energy release of the slow component is small and the probability of fragment translational energy distribution decreases monotonically with the energy. It is the typical characteristic of dissociation from a molecule undergoes internal conversion to the ground electronic state with no exit barrier.

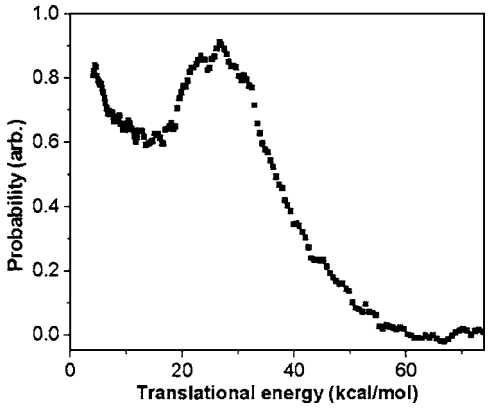

FIG. 5. Translational energy distribution of $C_8NH_7+h\nu(193$ nm$) \rightarrow C_8NH_6+H$.

The dissociation rate of the neutral excited indole molecules due to the 193 nm photon excitation was measured from the disk-like image intensity change of $m/e=89$ and 90 at various delay times. A dissociation rate of $(6\pm1)\times10^5$ s^{-1} was obtained, as shown in Figs. 6(a) and 6(b). The slow dissociation rate is ascribed to the dissociation from the ground electronic state. For $m/e=116$, a slow rise of the product growth sat on the top of a large signal was observed, as illustrated in Fig. 6(c). The slow rise shows the similar dissociation rate as that obtained from $m/e=89$ and 90. It must correspond to the dissociation from the ground electronic state. On the other hand, the large signal underneath the product growth must result from the disk-like image or a fast rise component that the rise is faster than our instrument time response, corresponding to the dissociation from the electronically excited state. A dissociation rate of $k=(6\pm1)\times10^5$ s^{-1} was obtained by fitting the data to the equation: $A_1+A_2\times\exp(-kt)+A_3\times(1-\exp(-kt))$. The first term represents the fast rise component, the second term represents the decay of the disk-like image, and the third term represents the slow rise component.

B. 248 nm

Ion images obtained at this wavelength are similar to that at 193 nm. As shown in Fig. 7(a), a line shape image of $m/e=116$ was obtained at 248 nm, indicating the H atom elimination channel. Since the photon energy is much smaller at 248 nm, the length of the image at 248 nm is shorter than that at 193 nm. Although the experimental delay time between pump and probe laser pulses is as long as 90 μs, the length of the image of $m/e=116$ is still very short due to the small available energy. It is difficult to totally separate the slow component from the interference of parent ion image even at such a long delay time. Therefore, we cannot determine the ratio between fast and slow components accurately. The probability of the slow component shown in Fig. 7(b) includes the interference from parent molecules. The slow component was estimated to be less than 25% of the fast component. The peak of the fast component is located at 15 kcal/mol, and the translational energy as much as 30 kcal/mol can be released. It reaches the maximum available energy of the reaction $C_8NH_7+h\nu(248$ nm$) \rightarrow C_8NH_6+H$. The distribution of the fast component indicates that it results from the electronically excited state.

IV. DISCUSSION

The aromatic amino acids and the nucleic acid bases are some of the most important molecules in biochemistry. One important photochemical characteristic of these molecules is the low quantum yields of fluorescence. These have been explained by the existence of very fast nonradiative processes which efficiently quench the excited state.[16,17] The

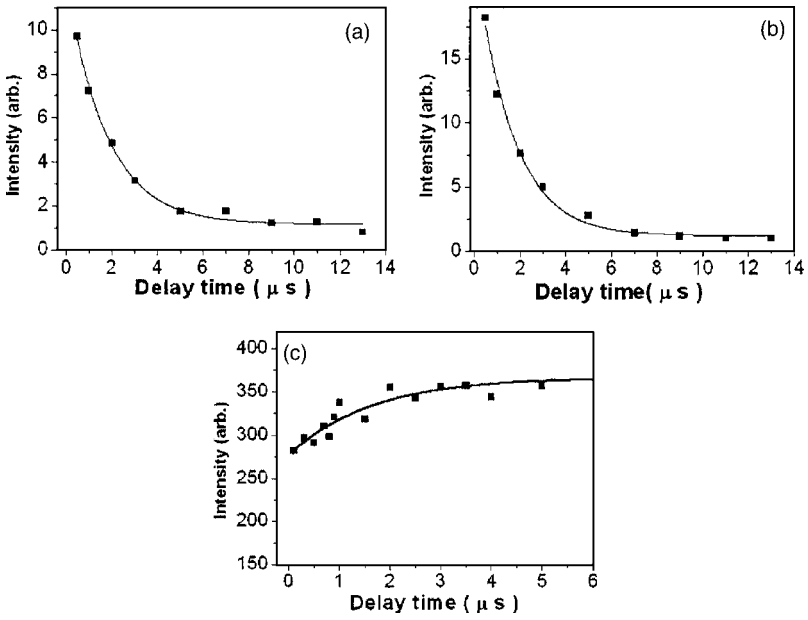

FIG. 6. Disk like ion image intensity decay (a) $m/e=89$, (b) $m/e=90$, (c) product growth of $m/e=116$ with respect to the delay time between pump and probe pulses. The solid squares represent experimental data, and the solid lines represent the fit to the equation $A\times\exp(-kt)$ for (a) and (b), and fit to the equation $A_1+A_2\times\exp(-kt)+A_3\times(1-\exp(-kt))$ for (c).

nonradiative processes presumably are ultrafast internal conversion (IC) back to the electronic ground state.[18] Following the internal conversion, they quickly dissipate the photon energy to solvent molecules by various energy transfer processes before more profound chemical rearrangements can take place. This so-called photostability is obviously particularly essential to protect these molecules from UV radiation.

Phenol and indole are the chromophores of the aromatic amino acid tyrosine and tryptophan, respectively. Recently *ab initio* calculations and experimental results have suggested a different nonradiative process for these two molecules.[10] Instead of internal conversion to the ground electronic state, H atom elimination through the dissociation of O–H and N–H bonds on a repulsive potential energy surface was suggested to be the other process after excitation to the S_1 state. Since the dissociation on the repulsive surface is very fast, it will not be quenched easily even in the condensed phase by the surrounding solvent molecules. The potential reactions of these molecules following the UV radiation must be considered if dissociation from the repulsive potential occurs.

For phenol, the minimum of the $S_1(\pi\pi^*)$ state is located at 4.5 eV above S_0,[19] and the $\pi\pi^*-\pi\sigma^*$ conical intersection is at ~5 eV. The internal conversion from S_1 to S_0 and intersystem crossing from S_1 to T_1 are the dominant decay channels for the phenol molecules after the excitation by 4.5 eV photons.[20] However, as the excitation photon energy increases to 5 eV, H atom elimination becomes the major channel even in the condensed phase. Photodissociation of phenol at 193 and 253 nm in the condensed phase studied by Fourier transform electron paramagnetic resonance and transient absorption spectroscopy shows that triplet state is not involved in the dissociation process.[21,22] The observation of large translational energy release of H atom elimination channel in phenol in our previous experimental measurement provides a direct evidence of the $\pi\pi^*-\pi\sigma^*$ predissociation mechanism of phenol at 248 nm.[23]

Although indole has been studied extensively, most of the studies focused on the spectroscopy and nonradiative decay rate, photodissociation of indole has received little attention. Our experimental measurement demonstrated that H atom elimination is the only dissociation channel of indole at 248 and 193 nm. The ratio between the fast and the slow components in the translational energy distribution changes from larger than 4.0 at 248 nm to 1.2 at 193 nm. The increase of the slow component with the increase of photon energy indicates that the internal conversion rate from the corresponding photoexcited state to the ground electronic state increases with the photon energy. The increase is likely due to the increase of the density of state at higher energy levels. Since there is no significant exit barrier of $C_8NH_7\rightarrow C_8NH_6+H$ in the ground electronic state, the fast component in the translational energy distribution must result from the dissociation in the excited electronic state. This excited state can be a state with a repulsive potential. It can also be the other excited state with a large exit barrier. For example,

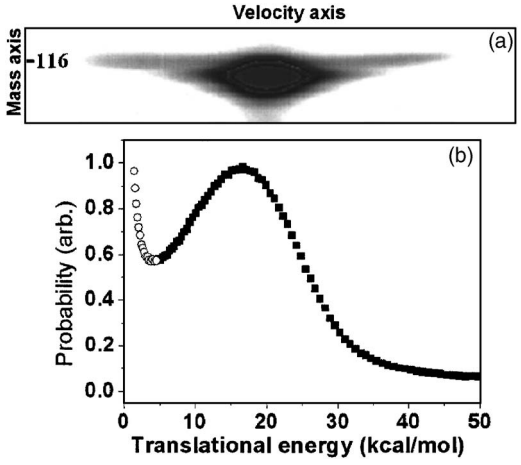

FIG. 7. (a) Ion image of $m/e=116$ at delay time 90 μs. (b) Translational energy distribution of $C_8NH_7+h\nu(248\text{ nm})\rightarrow C_8NH_6+H$. The solid squares represent the fast component, and open circles represent the maximum probability of slow component.

the triplet state might have an exit barrier.[24,25] Although the $\pi\sigma^*$ state with a repulsive potential suggested by the calculation is most likely the state that results in the fast component of translational energy, we can not completely exclude possibility of the other excited states at this moment due to the lack of the information of the other states.

ACKNOWLEDGEMENT

The work was supported by the National Science Council Taiwan, under contract NSC 93-2113-M-001-007.

[1] J. R. Platt, J. Chem. Phys. **19**, 101 (1951).
[2] B. J. Fender, D. M. Sammeth, and P. R. Callis, Chem. Phys. Lett. **239**, 31 (1995).
[3] L. A. Phillips and D. H. Levy, J. Chem. Phys. **85**, 1327 (1986).
[4] R. Bersohn, U. Even, and J. Jortner, J. Chem. Phys. **80**, 1050 (1984).
[5] G. A. Bickel, D. R. Demmer, E. A. Outhouse, and S. C. Wallace, J. Chem. Phys. **91**, 6013 (1989).
[6] N. Glasser and H. Lami, J. Chem. Phys. **74**, 6526 (1981).
[7] D. R. Demmer, G. W. Leach, and S. C. Wallace, J. Phys. Chem. **98**, 12834 (1994).
[8] C. Dedonder-Lardeux, D. Grosswasser, C. Jouvet, and S. Martrenchard, PhysChemComm **4**, 1 (2001).
[9] A. L. Sobolewski and W. Domcke, Chem. Phys. Lett. **315**, 293 (1999).
[10] (a) A. L. Sobolewski, W. Domcke, C. Dedonder-Lardeux, and C. Jouvet, Phys. Chem. Chem. Phys. **4**, 1093 (2002); (b) W. Domcke and A. L. Sobolewski, Science **302**, 1693 (2003); (c) K. Daigoku, S. Ishiuchi, M. Sakai, M. Fujii, and K. Hashimoto, J. Chem. Phys. **119**, 5149–5157 (2003); (d) G. A. Pino, C. Dedonder-Lardeux, G. Gregoire, C. Jouvet, S. Martrenchard, and D. Solgadi, J. Chem. Phys. **111**, 10747 (1999); (e) G. A. Pino, G. Gregoire, C. Dedonder-Lardeux, C. Dedonder-Lardeux, C. Jouvet, S. Martrenchard, and D. Solgadi, Phys. Chem. Chem. Phys. **2**, 893 (2000); (f) S. Ishiuchi, K. Daigoku, M. Saeki, M. Sakai, K. Hashimoto, and M. Fujii, J. Chem. Phys. **17**, 7077 (2002); (g) S. Ishiuchi, K. Daigoku, M. Saeki, M. Sakai, K. Hashimoto, and M. Fujii, J. Chem. Phys. **117**, 7083 (2002).
[11] B. C. Dian, A. Longarte, and T. S. Zwier, J. Chem. Phys. **118**, 2696 (2003).
[12] S. T. Tsai, C. K. Lin, Y. T. Lee, and C. K. Ni, Rev. Sci. Instrum. **72**, 1963 (2001).
[13] S. T. Tsai, C. K. Lin, Y. T. Lee, and C. K. Ni, J. Chem. Phys. **113**, 67 (2000).
[14] C. K. Lin, C. L. Huang, J. C. Jiang, H. Chang, S. H. Lin, Y. T. Lee, and C. K. Ni, J. Am. Chem. Soc. **124**, 4068 (2002).
[15] M. Jonsson, J. Lind, T. E. Eriksen, and G. Merenyi, J. Am. Chem. Soc. **116**, 1423 (1994).
[16] P. R. Callis, Annu. Rev. Phys. Chem. **34**, 329 (1983).
[17] D. Creed, Photochem. Photobiol., **537**, 39 (1984).
[18] A. Reuther, H. Iglev, R. Laenen, and A. Laubereau, Chem. Phys. Lett. **325**, 360 (2000).
[19] H. D. Bist, J. C. D. Brand, and D. R. Williams, J. Mol. Spectrosc. **24**, 413 (1967).
[20] A. Sur and P. M. Johnson, J. Chem. Phys. **84**, 1206 (1986).
[21] A. Bussandri and H. van Willigen, J. Phys. Chem. A **106**, 1524 (2002).
[22] R. Hermann, G. R. Mahalaxmi, T. Jochum, S. Naumov, and O. Brede, J. Phys. Chem. A **106**, 2379 (2002).
[23] C. M. Tseng, Y. T. Lee, and C. K. Ni, J. Chem. Phys. **121**, 2459 (2004).
[24] C. L. Huang, J. C. Jiang, S. H. Lin, Y. T. Lee, and C. K. Ni, J. Chem. Phys. **116**, 7779 (2002).
[25] C. L. Huang, J. C. Jiang, Y. T. Lee, and C. K. Ni, J. Chem. Phys. **117**, 7034 (2002).